J. Phys. B: At. Mol. Opt. Phys. **42** (2009) 065402 (9pp) doi:10.1088/0953-4075/42/6/065402

Robust carrier-envelope phase retrieval of few-cycle laser pulses from high-energy photoelectron spectra in the above-threshold ionization of atoms

Samuel Micheau[1], Zhangjin Chen[1], Toru Morishita[2,3], Anh-Thu Le[1] and C D Lin[1]

[1] J R Macdonald Laboratory, Physics Department, Kansas State University, Manhattan, KS 66506-2604, USA
[2] Department of Applied Physics and Chemistry, University of Electro-Communications, 1-5-1 Chofu-ga-oka, Chofu-shi, Tokyo 182-8585, Japan
[3] PRESTO, Japan Science and Technology Agency, Kawaguchi, Saitama 332-0012, Japan

Received 27 October 2008, in final form 8 February 2009
Published 9 March 2009
Online at stacks.iop.org/JPhysB/42/065402

Abstract
The two-dimensional momentum distributions of high-energy photoelectrons generated in the above-threshold ionization of atoms by intense laser pulses are analysed as resulting from the elastic backscattering of laser-induced returning electrons. Using this quantitative rescattering theory, we show that the returning electron wave packets are entirely determined by the properties of the laser pulses, including the absolute value of the carrier-envelope phase (CEP). We then present a robust method to precisely retrieve the absolute phase of few-cycle pulses by analysing separately the CEP dependence of the electron spectra emitted on the left and on the right directions along the laser polarization axis. In addition, our approach offers the possibility of measuring the laser peak intensity and pulse duration with an estimated error of a few per cent.

(Some figures in this article are in colour only in the electronic version)

1. Introduction

The electric field of a laser pulse can be written in general in the form of $E(t) = E_0(t)\cos(\omega t + \phi)$, where $E_0(t)$ is the amplitude, ϕ is the carrier-envelope phase (CEP) and $\omega/2\pi$ is the mean frequency. Recent advance in laser technology has made it possible to generate few-cycle pulses, such that the time variation of the electric field pulses can be controlled by manipulating the CEP [1]. For these very short pulses, experimental evidence of the influence of the absolute phase has been manifested in the emission direction of electrons from atoms [2], in high-harmonic generation (HHG) [3], in non-sequential double ionization yield [4] and in the asymmetric dissociative ionization of D_2 molecules [5, 6]. CEP-stabilized laser pulses have permitted the generation of attosecond pulses by means of HHG [7–9], and have a high potential for applications in many other fields such as the coherent control of molecular dynamics. However, while experimentally the relative CEP can be fixed, direct measurement of the absolute value of the CEP itself still relies on theoretical simulations.

Several techniques have been proposed to measure the absolute phase of few-cycle laser pulses. Apolonski *et al* [10] studied the photoemission dependence of a gold surface on the CEP and obtained a qualitative agreement with the simulations [11]. Recently, the observation of half-cycle cut-offs in HHG spectra has been used to retrieve the CEP [12]. However, most of CEP measurements, as well as theoretical works, have been so far based on the analysis of above-threshold ionization (ATI) electron spectra in the strong field ionization of atomic species [13–22]. One of the first measurements of the absolute phase was implemented by Paulus and coworkers [23], where the asymmetry of electrons emerging in the left versus in the right directions (or up versus down) is determined as the CEP is varied. The

absolute value of the CEP is evaluated by comparing the measured left–right asymmetry of the integrated high-energy ATI electrons against classical calculations. Subsequently, Tong *et al* [24] calculated the electron spectra from solving the time-dependent Schrödinger equation (TDSE). By comparing with the electron spectra measured in [23], it was concluded that the original experimental CEP should be shifted by 0.15π. A thorough discussion of the dependence of electron energy spectra on the CEP can be found in [25]. In this review, the authors describe the different methods employed to measure the CEP. For the stereo-ATI method, the confusing behaviour of the left/right total electron yield asymmetry on pulse duration, laser intensity and atomic species is emphasized, and the advantages of the high-energy electron dependence over the CEP are highlighted.

Recently, Kling *et al* [26] reported energy- and angle-resolved ATI spectra generated by phase-stabilized few-cycle pulses on argon, krypton and xenon atomic targets using the velocity-map imaging (VMI) technique, where electrons are projected onto a two-dimensional position-sensitive detector. The left–right asymmetry of the ATI spectra of Ar has been evaluated versus the kinetic energy of the photoelectrons and compared to calculations based on solving the TDSE and by using the strong field approximation. Since experimental electron spectra are always obtained over the laser focus volume, theoretical calculations have to be carried out with many laser intensities in order to generate electron spectra that can be directly compared to experiments. To carry out so many TDSE calculations becomes quite time consuming and not very practical. Furthermore, in a typical laser experiment, the peak laser intensity and pulse duration (measured in terms of the full width at half-maximum (FWHM) of the intensity) are also not accurately characterized. Thus, the calibration of the absolute CEP should be accompanied with the determination of the pulse duration and peak intensity. In a recent letter [27], we have proposed an alternative method of analysing the high-energy ATI electron (HATI) spectra. Using the data from Kling *et al* [26], we were able to show that the absolute CEP, the peak laser intensity and the pulse duration can be accurately retrieved to within a few per cent and that the retrieval method is very efficient.

To retrieve the absolute CEP, in [27], two renovations were suggested. First, instead of examining the left/right asymmetry of the electron spectra with the change of the CEP, the high-energy peak or the cut-off energy of the left or of the right electron spectra (integrated over 10° about the polarization axis) versus the CEP is examined. Second, the theoretical HATI electron spectra are calculated using the recently developed quantitative rescattering theory (QRS) [28–30]. Using the QRS, the calculations of HATI spectra speed up by a factor of few hundreds to thousands as compared to solving the TDSE, but with comparable accuracy. Thus, many repetitive calculations can be carried out to generate electron spectra (including volume integration) to identify laser parameters that best fit the experimentally measured spectra. The application of this new method for retrieving the laser parameters from the data of Kling *et al* has been presented in [27]. In this paper, we present the details of the theoretical analysis.

To make this paper self-contained, in section 2 we first summarize the recently developed QRS model. This model states that the HATI electron momentum spectra can be expressed as the product of a returning electron wave packet with the backscattered differential elastic scattering cross sections between the target ion and the *free* returning electrons. We will use a simplified version of this model where the returning electron wave packet is obtained from the second-order strong field approximation. In section 3 we show how the rescattering wave packet directly reflects the change of the CEP. This fact can then be used in section 4 as the basis for the new method of retrieving the CEP from the electron momentum spectra, including how the laser focus volume affects the electron energy spectra. Section 5 summarizes this paper.

2. Theoretical models for high-energy ATI electrons

2.1. High-energy ATI electrons and rescattering model

Considerable understanding of HATI spectra from atoms has been achieved since 1990s [31–33]. Qualitatively, they are understood based on the rescattering model [34, 35]. In this model, electrons that are released earlier by tunnelling ionization may be driven back by the laser field to recollide with the target ion. The plateau electrons are due to elastic large-angle backscattering of the returning electrons by the target ion [31–33]. This qualitative rescattering picture has been recently put in a quantitative form by us [28–30]. Based on accurate results by solving the TDSE, it has been demonstrated that the high-energy photoelectron momentum distribution $I(p,\theta)$ can be written in the form

$$I(p,\theta) = W(p_r)\sigma(p_r,\theta_r), \tag{1}$$

where $\sigma(p_r,\theta_r)$ is the elastic differential cross section (DCS) between 'free' electrons with the ion in the absence of the laser field. Here, p_r and θ_r are the momentum and the scattering angle of the 'incident' free electron, respectively, and $W(p_r)$ is interpreted as the returning electron wave packet (RWP) before it is backscattered. Equation (1) thus states that the dependence of the high-energy electron distribution over the laser parameters is solely included in the RWP. The momentum $\mathbf{p}$ (with magnitude p and angle θ with respect to the polarization axis) of the photoelectron is related to the momentum $\mathbf{p}_r$ right after backscattering by the vector potential $A_r\hat{\mathbf{p}}_z$ at the time of the collision via

$$\mathbf{p} = \mathbf{p}_r - A_r\hat{\mathbf{p}}_z. \tag{2}$$

Atomic units are used in the above equation and the rest of this paper unless otherwise noted. In the above equation, $A_r = A(t_r)$ is the instantaneous magnitude of the vector potential at the time t_r of the recollision, and the last term corresponds to the drift momentum the electron gains as it further propagates in the linearly polarized laser field (direction $\hat{\mathbf{p}}_z$) to the laser-free region. In terms of momentum components along the polarization direction and the direction perpendicular to it, equation (2) is written as

$$p\cos\theta = \pm p_r\cos\theta_r - A_r \tag{3}$$

$$p \sin\theta = p_r \sin\theta_r, \tag{4}$$

where the positive sign in equation (3) refers to the left side ($p < 0$) and the negative sign to the right side ($p > 0$) of the 2D momentum distribution. These equations show that high-energy electron momentum is obtained only when the electron is scattered into the backward direction where $\theta_r > 90^\circ$.

According to classical calculation for an electron in a monochromatic laser field [34], electrons which are tunnel ionized near the peak electric field and recollide with the ion core at a time where the vector potential is at its peak value, A_0, will have a maximum returning energy of $E_r = p_r^2/2 = 3.17U_p$ where the ponderomotive energy is $U_p = A_0^2/4$. Thus, the maximum returning electron momentum is $p_r = 1.26A_0$.

The validity of equation (1) was first established using $I(p,\theta)$ calculated from solving the TDSE for rare gas atoms within the single active electron approximation [30]. Experimentally, equation (1) has been used to extract the elastic scattering cross sections from laser-generated HATI spectra using long pulses (100 fs) [36] as well as short pulses (8 fs) [37], and the derived DCSs from the experiments were shown to be in good agreement with the theoretically calculated DCSs.

In actual experiments, the accurate value of A_0 is not generally known. By restricting $p_r = 1.26A_0$, the applicability of equation (1) is quite limited. In [29], equation (1) was extended to returning electrons which have momentum less than $1.26A_0$. In fact, for electrons which return to the parent ion with $A_r < A_0$, we relate the momentum p_r of the recolliding electrons to the vector potential A_r by $p_r = 1.26|A_r|$. For high-energy electrons beyond $10U_p$, we use $p_r = p - A_0$ since the maximum vector potential is A_0.

With these generalizations, we first check the validity of equation (1) using $I(p,\theta)$ calculated from solving the TDSE for a model one-electron atom in a laser field. The one-electron atom is described by a model potential $V(r)$. The differential cross section $\sigma(p_r,\theta_r)$ of a free electron with momentum p_r by such a potential $V(r)$ can be accurately calculated [38]. For each θ, one can extract a returning wave packet $W(p_r) = I(p,\theta)/\sigma(p_r,\theta_r)$. If equation (1) is valid, as has been shown for HATI electrons, then the extracted $W(p_r)$ should be independent of θ. Thus, we can then interpret $W(p_r)$ as the returning electron wave packet. Note that $W(p_r)$ is derived from photoelectron spectra at the end of the laser pulse; thus, it contains interference due to wave packets generated at different half cycles that end up with identical photoelectron momentum.

2.2. Second-order strong field approximation

Equation (1) which was established based on TDSE calculations confirms that accurate HATI spectra can indeed be written as the product of a RWP with the DCS between free electrons with target ions. To obtain a RWP, one still needs to solve the TDSE; thus, equation (1) itself does not save the computational effort. An alternative method is to calculate the HATI momentum spectrum using the second-order strong field approximation [39]. This theory is identical to the so-called improved strong field approximation used by Milošević and coworkers [40, 41]. Starting with the standard strong field approximation and including only the first two terms of the perturbation expansion, one can write the probability amplitude of detecting an electron with momentum $\mathbf{p}$ as

$$f(\mathbf{p}) = f^{(1)}(\mathbf{p}) + f^{(2)}(\mathbf{p}), \tag{5}$$

where the first term

$$f^{(1)}(\mathbf{p}) = -\mathrm{i}\int_{-\infty}^{\infty} \mathrm{d}t \langle \chi_{\mathbf{p}}(t)|H_i(t)|\Psi_0(t)\rangle \tag{6}$$

corresponds to the standard SFA, or SFA1, and the second term (SFA2) is

$$f^{(2)}(\mathbf{p}) = -\int_{-\infty}^{\infty}\mathrm{d}t\int_{-\infty}^{t}\mathrm{d}t'\int \mathrm{d}\mathbf{k}\langle\chi_{\mathbf{p}}(t)|V|\chi_{\mathbf{k}}(t)\rangle \times\langle\chi_{\mathbf{k}}(t')|H_i(t')|\Psi_0(t')\rangle. \tag{7}$$

In these expressions,

$$H_i(t) = \mathbf{r}\cdot\mathbf{E}(t) \tag{8}$$

is the laser–electron interaction, in length gauge and in dipole approximation, and the electric field $\mathbf{E}(t)$ of the laser pulse is chosen to be linearly polarized along the z-axis:

$$\mathbf{E}(t) = E_0 a(t)\cos(\omega t + \phi)\hat{z}, \tag{9}$$

where ϕ is the CEP. The envelope function is taken as

$$a(t) = \cos^2\left(\frac{\pi t}{T}\right) \tag{10}$$

for the time interval $(-T/2, T/2)$, and zero elsewhere, and T is the total duration of the pulse and is related to the FWHM of the intensity, or the pulse duration τ, by $\tau = T/2.75$. The functions $\chi_{\mathbf{p}}(t)$ are the usual Volkov states describing free electrons in the laser field and $\Psi_0(t)$ is the ground state wavefunction. In the numerical integration of $f^{(2)}(\mathbf{p})$, an additional damping factor $\mathrm{e}^{-\alpha r}$ is introduced in the model potential to avoid the singularity in the integrand. We choose $\alpha = 2$ and checked that the magnitude of $f^{(2)}$ slightly varies with this value, but not the shape. For HATI electrons, only the second term $f^{(2)}(\mathbf{p})$ is important. The integral is calculated within the saddle point approximation for the integration with respect to $\mathbf{k}$, as described in [42]. The electron momentum distribution is given by $I(p,\theta) = |f(\mathbf{p})|^2$.

2.3. Quantitative rescattering theory

In an earlier paper, Chen *et al* [39] showed that the HATI electron momentum spectrum calculated using SFA2 can also be written in a separable form as equation (1) except that the DCS is given by the first-order Born approximation. In figures 1(a) and (b), we compare the DCS calculated from exact quantum mechanical scattering waves and from the first Born approximation for electrons with momentum p_r colliding with the Xe^+ target. The DCS obtained from the first Born theory is clearly incorrect. In figures 1(c) and (d), we compare the RWP on the 'left' side obtained for a five-cycle laser pulse at a peak intensity of 1.0×10^{14} W cm^{-2} with a mean wavelength of 800 nm, and a CEP is equal to zero and $\pi/2$, respectively. One can see that the RWPs from SFA2 and from the TDSE are quite similar (the peak height from SFA2 has been normalized to the peak height from the TDSE), except

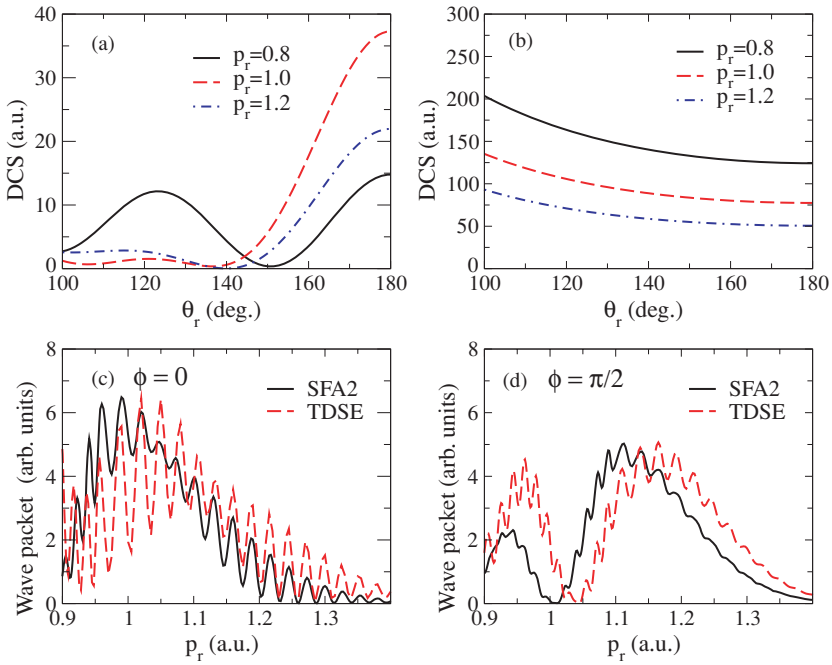

Figure 1. Elastic differential electron–ion scattering cross sections at large angles calculated using scattering waves (a) and first Born approximation (b) for Xe^+ and different incident momenta. Comparison of the 'left' returning wave packets extracted from the TDSE and SFA2 calculations for xenon atoms by a five-cycle laser pulse with a peak intensity of 1.0×10^{14} W cm^{-2} a mean wavelength of 800 nm, and a carrier-envelope phase sets to zero (c) and $\pi/2$ (d).

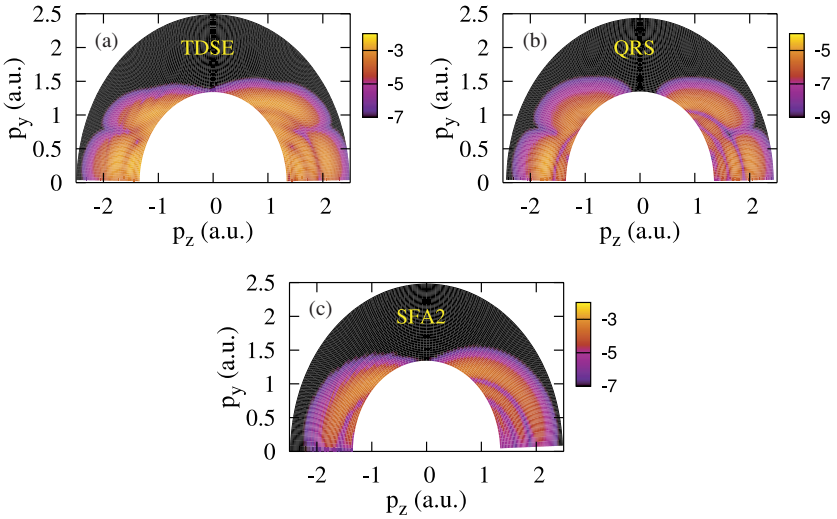

Figure 2. High-energy (above $4U_p$) photoelectron 2D momentum distribution (log-scale) calculated within the TDSE (a), the QRS theory (b) and SFA2 (c), for atomic xenon by a five-cycle laser pulse at a peak intensity of 1.0×10^{14} W cm^{-2} with a mean wavelength of 800 nm, and a carrier-envelope phase equals to zero.

that the RWP from SFA2 has a 4% shift to lower momentum. This shift is due to the neglect of the attractive interaction of the returning electron by the ion core in SFA2, with the main error coming from the neglect of the Coulomb interaction between the returning electron and the ion core. The good agreement between the two RWPs shows that the returning wave packet is dominated by the laser field, and this RWP can be conveniently calculated using SFA2. To simplify the computational effort, we thus proposed the quantitative rescattering theory (QRS) where we first calculate $I(p, \theta)$ using SFA2; we then replace the incorrect DCS from the first Born approximation by the 'exact' DCS calculated using quantum mechanical scattering waves. The validity of such an approach has been documented in [28, 29]. In figures 2(a) and (b), we compare the HATI spectra obtained from the QRS model with that from solving the TDSE directly. The two spectra indeed look very similar (on the logarithmic scale). On the other hand, the spectrum from SFA2 is not adequate (see figure 2(c)). We mention that the computer time for solving the TDSE is a few hundred to thousand times longer than for SFA2, for each set of laser parameters. Using the QRS model, we obtain HATI spectra with accuracy comparable to that from the TDSE but with

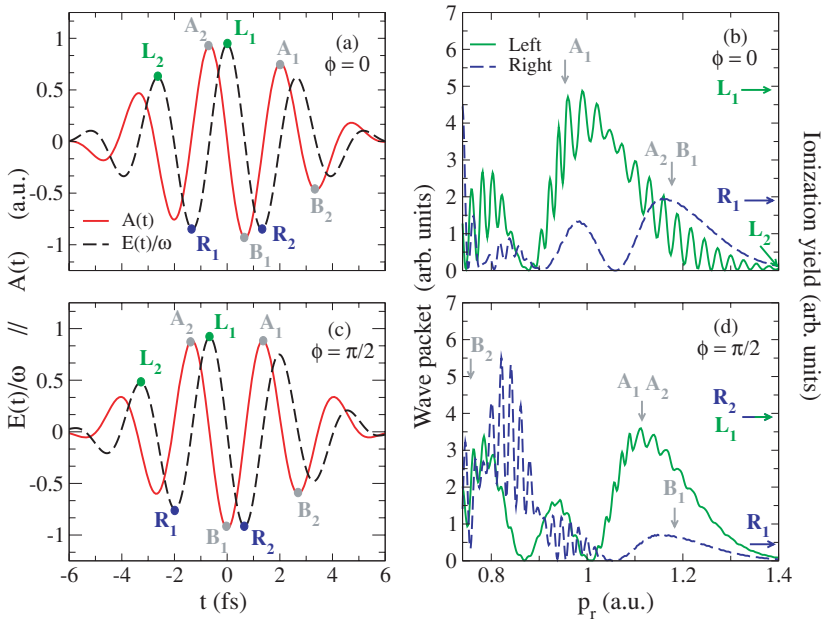

Figure 3. Temporal evolutions of electric fields and vector potentials for five-cycle laser pulses at a peak intensity of 1.0×10^{14} W cm^{-2}, with a wavelength of 800 nm, and carrier-envelope phases of $\phi = 0$ (a) and $\phi = \pi/2$ (c). Electron wave packets extracted from SFA2 for the left and right sides for $\phi = 0$ (b) and $\phi = \pi/2$ (d). In (b) and (d), the vertical arrows indicate the expected peak electron momenta when the electrons return to the corresponding peak vector potentials shown by identical labels in (a) and (c). The horizontal arrows indicate the relative tunnel ionization rates when electrons are ionized near the peak electric fields shown by identical labels in (a) and (c).

great saving in computer time. In fact, we can further improve the QRS by empirically shifting the RWP to higher momentum by a few per cent. Besides simplifications in the calculations, the QRS model states that for the relative yields of the HATI electrons, all the nonlinear laser properties are contained in the RWP which can be easily calculated from the second-order strong field approximation, while the structure factor of the target atom is all contained in the differential elastic scattering cross sections. The target structure will affect the RWP only through an overall normalization due to the dependence of the tunnelling ionization rate on the binding energy and wavefunction of the initial state.

3. CEP dependence of the wave packets and electron spectra

According to the QRS theory, the relative RWP contains all the information about the laser parameters. We thus analyse how the RWP depends on the CEP. In figures 3(a) and (c) we show the scaled electric field and vector potential of a five-cycle pulse, for a mean wavelength of 800 nm, for $\phi = 0$ (a cosine pulse) and $\phi = \pi/2$ (a sine pulse), respectively. In each case, the peak positions of the electric field and the vector potential are labelled. According to the classical theory, electrons that are released by tunnel ionization near the peak electric field of each half-cycle of a laser may return to the ion about three quarters of an optical cycle later, when the electric field is near zero or when the vector potential is near the peak. Quantum mechanically, we thus expect a wave packet whose strength is related to the magnitude of the peak electric field, and the electron's momentum is related to the peak vector potential at the time of return. In figure 3(b) we show the wave packets on the 'left' and on the 'right' sides calculated for $\phi = 0$ from the QRS model or, equivalently, from SFA2. In figure 3(b), the arrows labelled A_i and B_i ($i = 1, 2$) indicate the expected peak momenta of electrons according to $p_r = 1.26|A_r|$, where A_r is the corresponding peak vector potentials shown by identical labels in figure 3(a). Note that B_2 would appear outside the range of the figure. In figure 3(b), the horizontal arrows (L_1, L_2, R_1) indicate the relative tunnelling ionization rates when electrons are ionized near the peak electric fields, shown by identical labels in figure 3(a).

We comment that the wave packets shown in figure 3(b) are 'derived' from the photoelectron spectra at the end of the laser pulse; thus, electrons generated from different half-cycles may interfere if they have the same momentum. Consider the outermost peak of the right RWP; it shows no interference since only electrons which return to the core near B_1 can reach such high momentum. For the 'left' RWP, oscillations appear because electrons released near L_2 and L_1 and returning at A_2 and A_1, respectively, may interfere. Since the ionization yield near L_2 is much smaller, no significant peak appears near A_2 in the left RWP, except for contributing to the interference features.

The same analysis can be applied to identify the outermost peaks of the left and right RWPs for the sine pulse, as shown in figures 3(c) and (d).

We also note that there are secondary peaks that cannot be identified with the peak vector potentials, e.g. the second outermost peak in each wave packet. These secondary peaks are due to the interference of electrons following short and

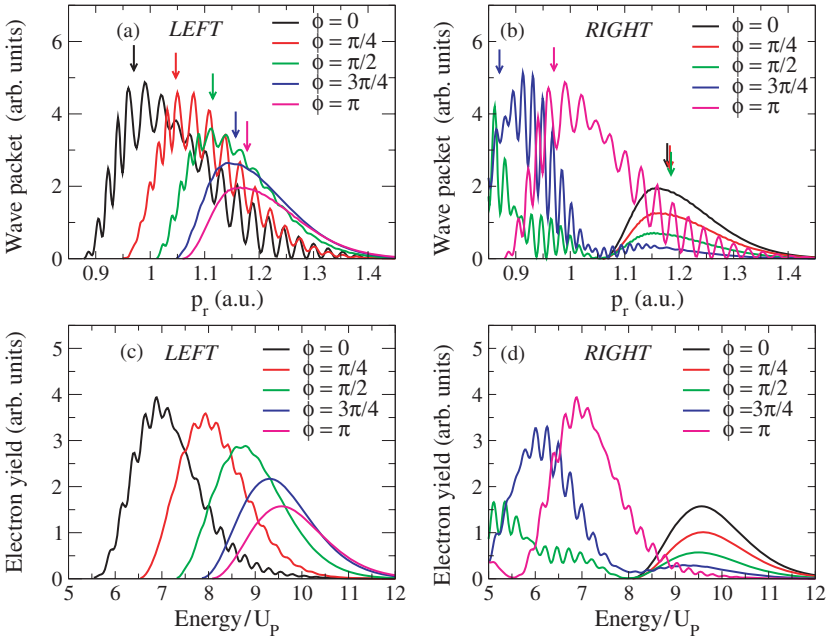

Figure 4. Electron wave packets extracted from the left (a) and right (b) sides for a laser pulse with a peak intensity of 1.0×10^{14} W cm^{-2}, pulse duration of five cycles, mean wavelength of 800 nm and different carrier-envelope phases. The arrows indicate the expected peak momenta from the peak vector potentials of the half-cycles responsible for the wave packet for the different absolute phases. (c), (d) Corresponding high-energy photoelectron spectra determined by means of the QRS model for xenon atoms. The spectra are calculated by integrating over a cone of 10° along the laser polarization axis.

long trajectories (in the classical context) which have been examined extensively in the context of high-order harmonic generation. For the CEP analysis, we usually focus only on the outermost peak of each wave packet.

From the above examples it is clear that the momentum distribution of the RWP evolves smoothly with the change of the CEP, as shown in figures 4(a) and (b), where only the outermost portion of each wave packet is displayed. For each of the left wave packets displayed in figure 4(a), the value of the peak momentum increases smoothly with the CEP, but the strength of the peak decreases. However, the peak positions for the last two CEPs at $\phi = 0.75$ and 1.0π do not change much, meaning a loss of accuracy if one would like to retrieve the CEP from such data. However, for the CEP in this region, the peak positions on the right wave packets change rapidly with an increase of the CEP (see figure 4(b)). Due to the symmetry, a shift of π in the CEP would induce the same results, but the left and right sides are interchanged. In figures 4(a) and (b), we show with arrows the peak momentum obtained from $p_r = 1.26|A_r|$, where A_r is the peak vector potential of the half-cycle which is responsible for the wave packet with the CEP indicated. For the outermost peak, they agree well with the actual wave packet extracted from the QRS model. This is similar to the half-cycle cut-off observed in the HHG spectra from few-cycle pulses [12].

Since the RWP is not measured directly in experiments, one has to retrieve the CEP from the electron momentum spectra. Instead of examining the whole 2D electron momentum spectrum, in figures 4(c) and (d) we compare the electron yield integrated over an angular range of 10° around the polarization axis, for electrons detected on the 'left' and the 'right', where the electron momentum spectra $I(p, \theta)$ were calculated using the QRS model. Note that the electron spectra resemble the RWPs with a clear shift of the peak momentum position as the CEP is varied.

4. Retrieval of the absolute CEP phase

4.1. Single intensity spectra

Using electron spectra similar to figures 4(c) and (d), we show in figure 5(a) how the peak position of the electron energy spectra integrated over 10° along the polarization axis changes with the pulse duration. Clearly the slope is quite steep for the short pulse and much flatter for the long pulse, as shown for pulses with an FWHM of 4.9, 6.5 and 8.0 fs, respectively. These curves are obtained from the electron spectra on the 'left' using Xe atoms as the target, with lasers of a mean wavelength of 800 nm, and electron energies are expressed in units of U_p. In figure 5(a), we note that for a CEP close to π, the curves are quite flat. It becomes more difficult to read out the CEP from the electron spectra on the 'left'. However, if the peak positions are read from the 'right' wave packet, as shown in the lower right of figure 5(a), the slope becomes steeper and thus a precise CEP can be retrieved. In figure 5(a), the CEP is shown only for the range of 0 and π. Clearly, for a CEP between π and 2π, the curves shown in figure 5(a) repeat except that 'left' and 'right' are interchanged.

In figure 5(b), we present the peak energies, normalized to U_p, as a function of the CEP for a five-cycle laser pulse and two intensities. The normalized peak positions are shown to be independent of the intensity such that the slope of the peak

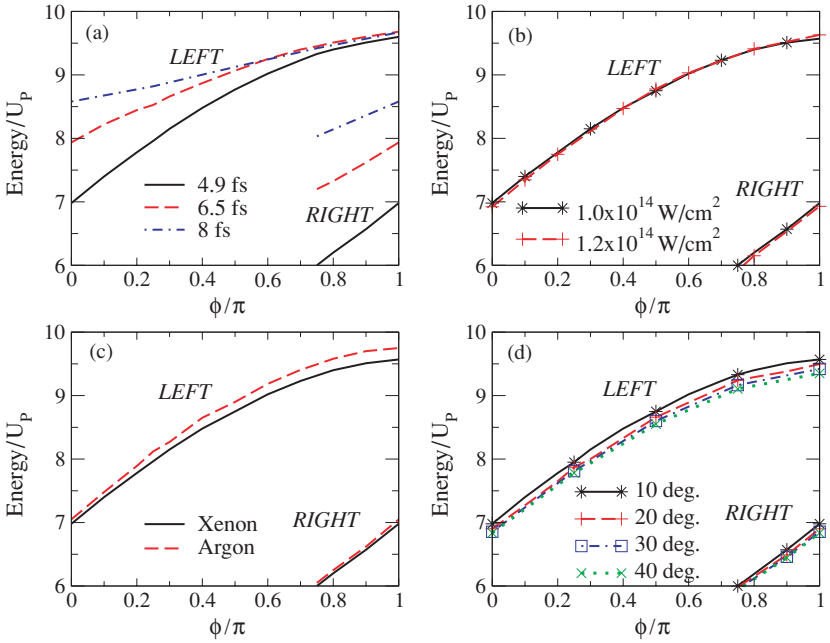

Figure 5. Left and right peak energies (normalized to U_p) as a function of the carrier-envelope phase: (a) for xenon atoms by an 800 nm laser pulse with a peak intensity of 1.0×10^{14} W cm^{-2} and different pulse durations, (b) for xenon atoms by a five-cycle laser pulse with a mean wavelength of 800 nm and different peak intensities, (c) for xenon and argon atoms by a laser pulse with a 4.9 fs pulse duration and other parameters as in (a). (d) Peak positions for different ranges of angular integration. The parameters are identical to figure 4(c) for xenon atoms.

energies versus the CEP is governed by the pulse duration only. As the momentum of the returning wave packet scales with the vector potential, the peak positions are indeed expected to scale with U_p.

According to the QRS, the RWP is essentially independent of the target if the same laser parameters are used. Since the peak energies are governed by the peak momentum of the wave packets, we thus expect the peak positions to be nearly independent of the target used. This is the case as illustrated in figure 5(c) for Xe and Ar atoms. Finally, while the peak position of the electron spectra varies slightly with the range of angular integration, the slope of the peak position versus the CEP stays the same (see figure 5(d)).

The results from figure 5 clearly indicate that the relative shift of the peak electron energy depends on the absolute CEP of the laser pulse. The amount of shift depends on how the envelope function of the vector potential changes as the CEP of the laser is changed. Thus the behaviour of the slopes shown in figure 5(a) is very general, independent of the target, peak intensity or the mean wavelength, if the electron energy is scaled with respect to U_p and the FWHM of the laser is scaled with respect to the optical period. We comment that analysing electron spectra from SFA2 calculations gives similar results, but the QRS model increases the accuracy of the method.

In figure 5 we follow the peak position of the electron spectra from the left or from the right sides separately, instead of using the left/right asymmetry. This allows us to focus on quantities which evolve smoothly with the change of the CEP and for easy interpolation.

4.2. *Volume effects*

The above analysis relies on electron spectra generated by a single laser intensity. Experimentally, electron spectra are obtained from a focused laser beam, with the intensity varying in space. Thus to retrieve the CEP from experimental data, theoretical calculations must be carried out to account for the volume integration [43, 44]. Assuming a Gaussian spatial distribution of the laser intensity, the volume of an isointensity shell is given by

$$V = \pi z_R w_0^2 \left[\frac{4(c_1 - c_2)}{3} + \frac{2\left(c_1^3 - c_2^3\right)}{9} - \frac{4}{3}[\tan^{-1}(c_1) - \tan^{-1}(c_2)] \right], \quad (11)$$

where $2w_0$ is the $1/e$ diameter of the focal spot, $z_R = \pi w_0^2/\lambda$ is the Rayleigh range of the focus and $c_j = [(i_0 - I_j)/I_j]^{1/2}$, with I_0 being the laser peak intensity and I_j the intensity of the shell j. In figures 6(a) and (b), we show the volume-integrated high-energy photoelectron spectra on the left and right sides (integrated over 10° along the polarization axis) for a peak intensity of 1×10^{14} W cm^{-2}, and the other parameters as in figures 4(c) and (d). Although the contrast is less pronounced when volume effects are included, the shift of the peak energy with the CEP clearly persists. Thus, the method presented in the previous section can still be safely used to accurately determine the absolute value of the CEP from volume-integrated theoretical or experimental data [27].

We performed similar calculations for argon atoms. The volume-integrated photoelectron spectra are shown in

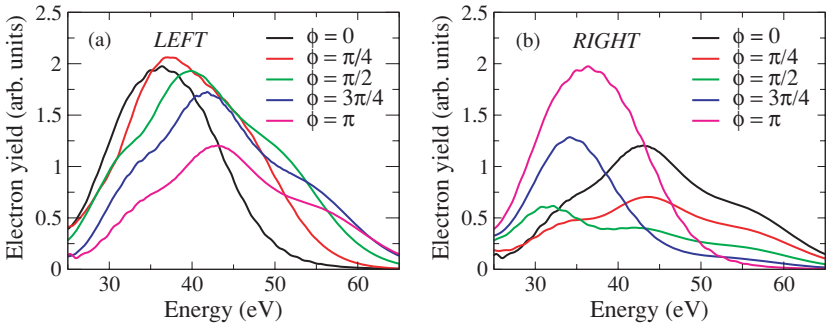

Figure 6. Left (a) and right (b) high-energy photoelectron spectra integrated over the interaction volume as a function of the carrier-envelope phase for xenon atoms by a five-cycle laser pulse with a peak intensity of 1.0×10^{14} W cm^{-2} and a mean wavelength of 800 nm. The spectra are from integrating over 10° along the laser polarization axis.

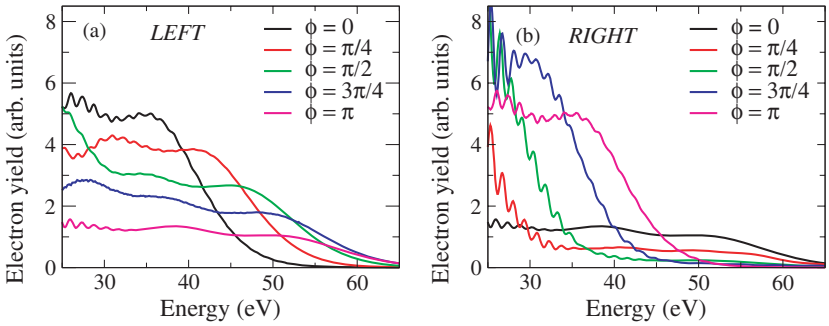

Figure 7. Left (a) and right (b) volume-integrated high-energy photoelectron spectra as a function of the CEP for argon atoms by a 800 nm five-cycle laser pulse with a peak intensity of 1×10^{14} W cm^{-2}. The spectra are from integrating over 10° along the laser polarization axis.

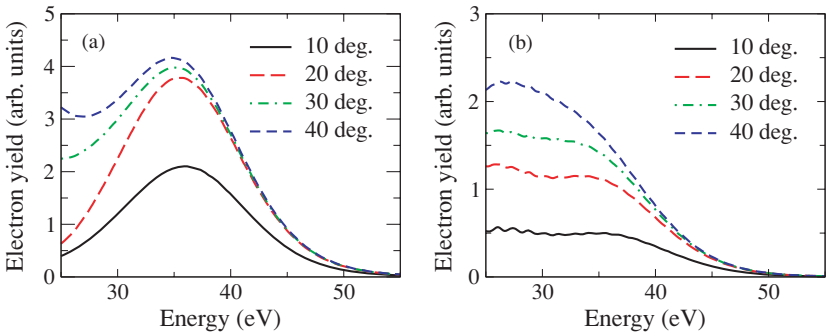

Figure 8. Volume-integrated high-energy photoelectron spectra on the left side for xenon (a) and argon (b) atoms for different angular ranges of integration along the laser polarization axis. The laser peak intensity is 1×10^{14} W cm^{-2} with a pulse duration of five cycles and a wavelength of 800 nm. The CEP is set to zero.

figures 7(a) and (b) as a function of the CEP for the left and right sides. Unlike the xenon results, the high-energy argon spectra (integrated over 10° around the polarization axis) do not display clean maximum, but each spectrum shows a clear cut-off. By analysing the change of the cut-off energy versus the CEP, the absolute phase of the laser pulse can be retrieved. The results in figures 6 and 7 were obtained for electrons integrated over 10° around the polarization axis. In figure 8, we show how the electron spectra change with the angle of integration for CEP = 0. For the Xe target, the peak position remains quite pronounced for an angular integration range from 10 to 40°. For the Ar target, the cut-off energy is more pronounced for an angular integration range from 10 to 20°. For larger angles, the cut-off energy becomes less clear. For the purpose of retrieving the CEP of the laser pulses, the xenon atom is clearly a better target.

5. Conclusions

In conclusion, we have studied the two-dimensional momentum distribution spectra of high-energy photoelectrons in the above-threshold ionization of atoms by few-cycle laser pulses. We have shown that the momentum distributions can be described, on a quantitative basis, as the product of a laser-induced returning electron wave packet by the elastic differential cross section between the target ion and free electrons. Thanks to this quantitative rescattering theory, we have demonstrated a robust method to accurately retrieve the

absolute phase of few-cycle laser pulses. Our method relies on the analysis of high-energy photoelectron spectra emitted in the left and in the right directions separately. We have shown that the yield and the peak energy of these electrons are determined by the laser's electric field and its vector potential, respectively, such that the shift of the peak energy with the carrier-envelope phase can be analysed to determine the absolute CEP. Furthermore, the quantitative rescattering theory is much more efficient than TDSE calculations in that it allows a rapid and accurate determination of the peak energies (or cut-off energies); thus, a laser focus volume effect can be included in the simulation in order to compare with experimental spectra. As demonstrated recently [27], this method provides an appealing tool to precisely determine the laser peak intensity, pulse duration and the absolute CEP phase simultaneously, with an expected error of a few per cent.

Acknowledgments

This work was supported in part by Chemical Sciences, Geosciences and Biosciences Division, Office of Basic Energy Sciences, Office of Science, US Department of Energy. TM is also supported by a Grant-In-Aid for Scientific Research (C) from the Ministry of Education, Culture, Sports, Science and Technology, Japan, and by the Japanese Society for the Promotion of Science (JSPS) Bilateral joint program between the US and Japan.

References

[1] Baltuška A *et al* 2003 *Nature* **421** 611
[2] Paulus G G, Grasbon F, Walther H, Villoresi P, Nisoli M, Stagira S, Priori E and De Silvestri S 2001 *Nature* **414** 182
[3] Nisoli M, Sansone G, Stagira S, De Silvestri S, Vozzi C, Pascolini M, Poletto L, Villoresi P and Tondello G 2003 *Phys. Rev. Lett.* **91** 213905
[4] Liu X *et al* 2004 *Phys. Rev. Lett.* **93** 263001
[5] Kling M F *et al* 2006 *Science* **312** 246
[6] Tong X M and Lin C D 2007 *Phys. Rev. Lett.* **98** 123002
[7] Kienberger R *et al* 2004 *Nature* **427** 817
[8] Mashiko H, Gilbertson S, Li C, Khan S D, Shakya M M, Moon E and Chang Z 2008 *Phys. Rev. Lett.* **100** 133906
[9] Sansone G *et al* 2006 *Science* **314** 443
[10] Apolonski A *et al* 2004 *Phys. Rev. Lett.* **92** 073902
[11] Lemell C, Tong X M, Krausz F and Burgdörfer J 2003 *Phys. Rev. Lett.* **90** 076403
[12] Haworth C A, Chipperfield L E, Robinson J S, Knight P L, Marangos J P and Tisch J W G 2007 *Nature Phys.* **3** 52
[13] Verhoef A J, Fernández A, Lezius M, O'Keeffe K, Uiberacker M and Krausz F 2006 *Opt. Lett.* **31** 3520
[14] Cormier E and Lambropoulos P 1998 *Eur. Phys. J.* D **2** 15
[15] Dietrich P, Krausz F and Corkum P B 2000 *Opt. Lett.* **25** 16
[16] Chelkowski S and Bandrauk A D 2002 *Phys. Rev.* A **65** 061802(R)
[17] Milošević D B, Paulus G G and Becker W 2003 *Opt. Express* **11** 1418
[18] Chelkowski S, Bandrauk A and Apolonski A 2004 *Opt. Lett.* **29** 1557
[19] Chelkowski S, Bandrauk A D and Apolonski A 2004 *Phys. Rev.* A **70** 013815
[20] Peng L-Y and Starace A F 2007 *Phys. Rev.* A **76** 43401
[21] Peng P-Y, Pronin E A and Starace A F 2008 *New J. Phys.* **10** 025030
[22] Liao Q, Lan P, Yang Z and Li Y 2008 *Opt. Express* **16** 6455
[23] Paulus G G, Lindner F, Baltuška A, Goulielmakis E, Lezius M and Krausz F 2003 *Phys. Rev. Lett.* **91** 253004
[24] Tong X M, Hino K and Toshima N 2006 *Phys. Rev.* A **74** 031405(R)
[25] Milošević D B, Paulus G G, Bauer D and Becker W 2006 *J. Phys. B: At. Mol. Opt. Phys.* **39** R203
[26] Kling M F, Rauschenberger J, Verhoef A J, Hasović E, Uphues T, Milošević D B, Muller H G and Vrakking M J J 2008 *New J. Phys.* **10** 025024
[27] Micheau S, Chen Z, Le A T, Rauschenberger J, Kling M F and Lin C D 2009 *Phys. Rev. Lett.* **102** 073001
[28] Chen Z, Le A T, Morishita T and Lin C D 2009 *Phys. Rev.* A in press
[29] Chen Z, Le A T, Morishita T and Lin C D 2009 *J. Phys. B: At. Mol. Opt. Phys.* **42** 061001
[30] Morishita T, Le A T, Chen Z and Lin C D 2008 *Phys. Rev. Lett.* **100** 013903
[31] Yang B, Schafer K J, Walker B, Kulander K C, Agostini P and Di Mauro L F 1993 *Phys. Rev. Lett.* **71** 3770
[32] Paulus G G, Becker W, Nicklich W and Walther H 1994 *J. Phys. B: At. Mol. Opt. Phys.* **27** L703
[33] Walker B, Sheehy B, Kulander K C and Di Mauro L F 1996 *Phys. Rev. Lett.* **77** 5031
[34] Corkum P 1993 *Phys. Rev. Lett.* **71** 1994
[35] Paulus G G, Nicklich W, Xu H, Lambropoulos P and Walther H 1994 *Phys. Rev. Lett.* **72** 2851
[36] Okunishi M, Morishita T, Prumper G, Shimada K, Lin C D, Watanabe S and Ueda K 2008 *Phys. Rev. Lett.* **100** 143001
[37] Ray D *et al* 2008 *Phys. Rev. Lett.* **100** 143002
[38] Schiff L I 1968 *Quantum Mechanics* 3rd edn (New York: McGraw-Hill) p 145
[39] Chen Z, Morishita T, Le A T and Lin C D 2007 *Phys. Rev.* A **76** 043402
[40] Milošević D B, Paulus G G and Becker W 2003 *Opt. Express* **11** 1418
[41] Gazibegović-Busuladžić A, Milošević D B and Becker W 2004 *Phys. Rev.* A **70** 053403
[42] Lewenstein M, Kulander K C, Schafer K J and Bucksbaum P H 1995 *Phys. Rev.* A **51** 1495
[43] Augst S, Meyerhofer D D, Strickland D and Chin S L 1991 *J. Opt. Soc. Am.* B **8** 858
[44] Morishita T, Chen Z, Watanabe S and Lin C D 2007 *Phys. Rev.* A **75** 023407